VII International Conference on Computational Methods for Coupled Problems in Science and Engineering
COUPLED PROBLEMS 2017
M. Papadrakakis, E. Oñate and B. Schrefler (Eds)

PHASE-FIELD MODELLING OF TERNARY EUTETIC SOLIDIFICATION IN HOT DIP GALVANIZATION

J.P. MOGERITSCH[1], A. LUDWIG[1], B. BÖTTGER[2], G. ANGELI[3], C.K. RIENER[3], R. EBNER[4]

[1] Chair of Simulation and Modelling of Metallurgical Processes, University of Leoben, Franz-Josef-Str. 18, A-8700 Leoben, Austria
e-mail: johann.mogeritsch@unileoben.ac.at, web page: https://www.unileoben.ac.at/
[2]ACCESS Materials & Processes, Intzestr 5, D- 52072 Aachen, Germany
[3]voestalpine Stahl GmbH, voestalpine-Straße 3, A-4020 Linz, Austria
[4]Material Center Leoben Forschungs GmbH, Roseggerstraße 12, 8700 Leoben

Key words: Phase-field modelling, hot dip galvanization, solidification, Zn-Al-Mg alloys

Abstract. Continuous hot dip galvanizing is one of the commercially most important process techniques used for protecting steel sheets against corrosion. Preheated steel sheets are continuously drawn through a pot with a molten zinc alloy. After passing a gas jet that controls the layer thickness multiple cooling units act to cool down the sheet. During passing these aggregates nucleation, dendritic primary solidification and the formation of a binary and ternary eutectic occurs. In the present paper, the coupled modelling of macroscopic heat flow, multiphase thermodynamics and crystal growth during solidification of a Zn-2.5 wt.% Al-1.5 wt.% Mg alloy is presented. The heat flow problem requires a numerical domain in the order of meters, growth of primary Zn-dendrites in the order of several hundred micrometers, and the interdendritic eutectic in the order of several nanometers. For technical alloys like the ternary system considered here, a thermodynamic database has been online linked to a phase-field model to describe phase transformations including all occurring solid/liquid or solid/solid interfaces. Process simulations have been used for getting appropriate thermal boundary conditions for 3D phase field simulations which were performed at three different length-scales. For modelling primary dendritic Zn-a seed density model was used for predicting the grain structure within the Zn layer. At a smaller length-scale, a small part of a Zn-dendrite surface was taken as starting point for simulating the transition between primary binary eutectic and ternary eutectic coupled growth of Zn-rich, Al-rich, and $MgZn_2$-phases. Finally, the morphology of the ternary eutectic has been evaluated at the smallest length scale. The comparison with real solidification microstructure reveals encouraging agreements.

1 INTRODUCTION

One of the most important material worldwide is steel, used in building, construction and motor vehicle industry. Unfortunately, many steel grades corrode which causes a substantial economic damage especially for the car industry. Demands to reduce this problem and to increase the service life cycle of steel leads to galvanizing, a very effective and low coast solution. Today, the most important production process for these coatings is the continuous hot-dip galvanizing process (or Sendzimir process).

The protection of steel against corrosion takes place at galvanizing plants with an alloy based on the Zn-Al(-Mg)-system [1-3]. Such continuous production plants consist of several different sections connected in series (Fig. 1). In the entry section the steel coils are trailed by welding before the now continuously steel sheet is cleaned and annealed within a furnace. Heating up closely above the zinc pot temperature the sheet is pulled into the galvanizing section through the liquid zinc alloy (~ 450 °C). Here, first a strong boundary layer of Fe-Al is formed on the steel sheet surface. This layer cares for a firmly adhered liquid zinc layer as soon as the sheet moves out of the bath and toward the cooling tower. Immediately after the zinc bath, the desired coating thickness is adjusted by air "knifes". Hereafter, the remaining liquid layer solidifies within the cooling tower and forms the characteristic microstructure for Zn-Al(-Mg) alloys. Finally, the zinc protected steel sheet is again portioned in coils at the exit section and prepared for further processing.

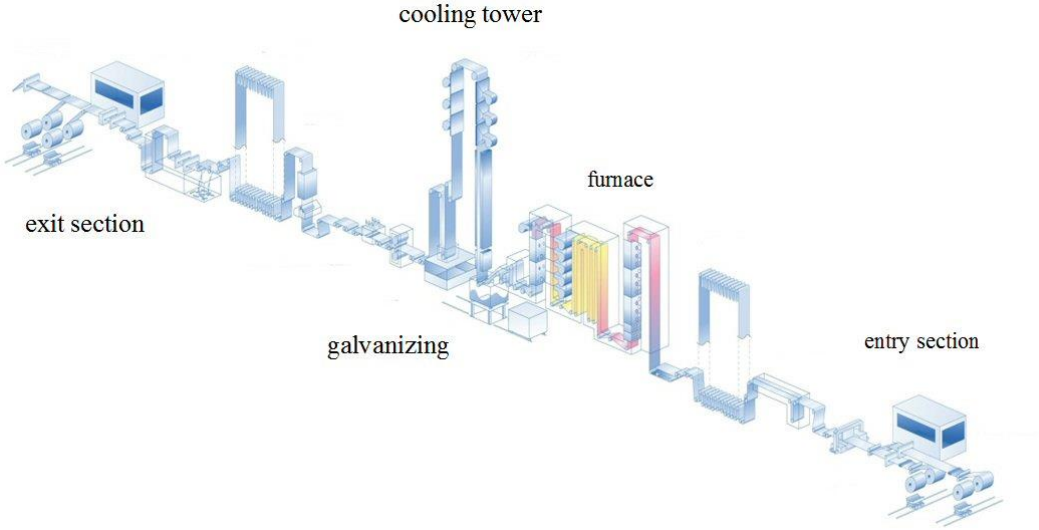

Figure 1: Hot dip galvanizing line at voestalpine Stahl, Linz [4]

The microstructure of the solidified Zn-Al(-Mg) alloy coating consists of primary zinc dendrites and interdendritic binary and ternary eutectics. The binary eutectic consists of the zinc phase combined with either the Laves phase ($MgZn_2$-phase), or the aluminum phase (Al-phase) depending on the bath composition [5]. At room temperature the primary fcc-Al phase decomposed into a secondary fcc-Al phase and a secondary hcp-Zn phase. The ternary eutectic is composed of Zn-, Al- and $MgZn_2$-phase [6-8]. According to [9, 10], in coatings the Mg-

Zn phase in the ternary eutectic is the $MgZn_2$-phase instead of the thermodynamically most stable Mg_2Zn_{11}-phase. In fact, only at cooling rates [11, 12] below or above the typical industry relevant process condition the Mg_2Zn_{11}-phase forms. It has also to be mentioned that the $MgZn_2$-phase forms not only as part of the eutectic, but also as hexagonal precipitates on further cooling to room temperature [6].

Phase-field models have become very popular for the simulation of microstructure evolution during alloy solidification processes. While early approaches rely on idealized descriptions of the phase diagrams [13, 14], more recent models which use thermodynamic databases [15] together with software tools for Gibbs energy minimization [16, 17] and allow for a more realistic description of multicomponent alloy solidification. The software MICRESS[1] is based on the phase-field concept for multiphase systems [16, 18] and allows for direct coupling to thermodynamic databases via the TQ Fortran interface to Thermo-Calc[2]. The software has been applied to a variety of alloy systems including 3D-simulations of Mg-Al dendrites [19] and a ternary eutectic model system [20].

In the present paper, numerical investigations on the formation of typical coating microstructure pattern for Zn-2.5 wt.% Al-1.5 wt.% Mg alloys are presented. The numerical investigations were done in parallel with experimental studies on laboratory prepared coated steel sheet samples.

2 EXPERIMENTAL PROCEDURE

The experimental procedure comprised the instrumented production of coatings with a galvanizing simulation device called GalvaSim [21], the investigation of the zinc coating with a scanning electron microscope (SEM) to obtain the microstructure, and the evaluation of key features to evaluate the numerical investigations.

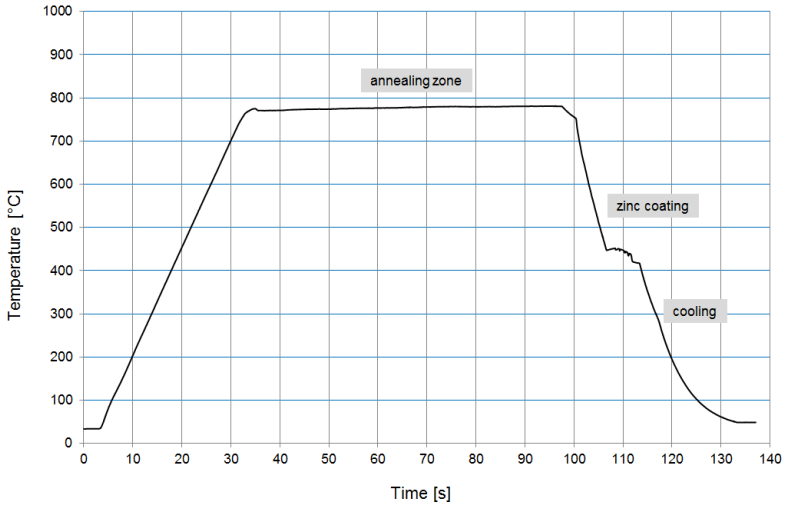

Figure 2: Example of a heat and cooling cycle measured at the galvanizing simulation device GalvaSim.

[1] MICRESS® software: http//:www.micress.de
[2] Thermo-Calc® software: http//:www.thermocalc.se

The voestalpine possesses with GalvaSim a device which allows reproducing the important process steps of a hot-dip-galvanizing process line in an instrumented and controlled way. The simulator consists of an annealing, galvanizing and skin passing section, assembled in vertical arrangement. Samples of different steel grades with various thicknesses and different heating and cooling procedure were coated with numerous Zn-Al(-Mg) alloys. For this work, a 0.75 mm thick DX53 steel sheet was coated with an Zn-2.5 wt.% Al-1.5 wt.% Mg layer of different thicknesses ranging from 10 µm to 100 µm. The applied heating and cooling cycle is shown in Fig. 2.

Small sections of the sample were prepared for SEM investigations. Fig 3 shows corresponding results. The coating surface with the primary dendrites and the surrounding ternary eutectic phase can be seen in Fig. 3a. The primary phase consists of the Zn-phase whereby the ternary eutectic composed of all three phases, Zn, Al and $MgZn_2$. If one compares the differences in length scale it is quite obviously that the size of the eutectic is more than one order of magnitude smaller than the dendritic phase. Also in cross-section the size difference is obvious (Fig. 3b). Additionally, it can be seen that the primary phase is completely surrounded by small Al-phase dots embedded in the $MgZn_2$-phase. It is randomly positioned in the coating layer, so that no clear statement about the actual nucleation positions can be made. The fine eutectic is enlarged shown in Fig. 3c. The structure shows three different phases which identifies the eutectic as being ternary. The eutectic consists of Zn- and $MgZn_2$-lamellae with Al-phase dots located along the $MgZn_2$-lamellae. Note that the Al-phase dot size is approximately equal to the $MgZn_2$-lamellae width. An investigation of the ternary eutectic reveals 44% of the area is covered with Zn-phase (bright), 28.7% with Al-phase (dark), and 27.3% with $MgZn_2$-phase (grey). Beside the ternary eutectic, quite rarely a binary eutectic (not shown here) was detected. This binary eutectic consist of the Zn- and Al-phase.

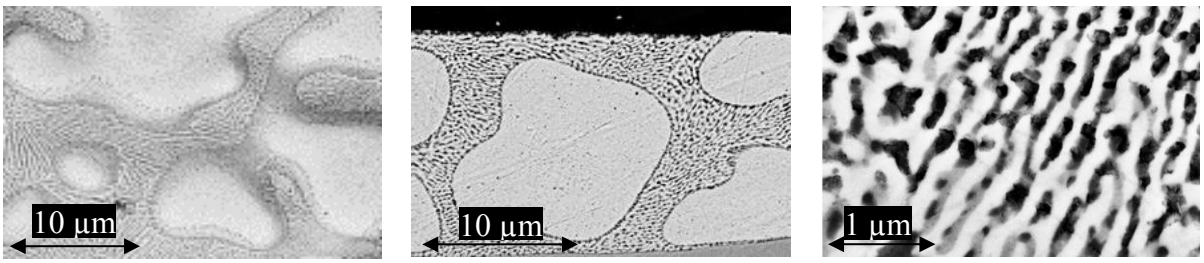

(a) (b) (c)

Figure 3: Microstructure of the investigated Zn-2.5 wt.% Al-1.5 wt.% Mg layer: (a) coating surface, (b) cross section, and (c) ternary eutectic. The Zn-phase appears bright, the $MgZn_2$-phase grey, and the Al-phase dark.

The evaluation of the microstructure revealed some key-features which had to be reproduced by the numerical investigations. This includes the occurrence and amount of the phases, the Al-phase dots surrounding the surface of the dendrites, and the morphological appearance of the ternary eutectic. In addition, the process conditions as measured from the GalvaSim coating device have to matched.

3 NUMERICAL INVESTIGATIONS

Numerical simulations of the solidification process and the microstructure formation were carried out by using Thermo-Calc, MICRESS, ANSYS-FLUENT[3] and Para View[4]. MICRESS was used to calculate the microstructure by a multiphase field method. ParaView visualize 3D results and was used to analyze the formation of the microstructure, with ANSYS-FLUENT we simulated the process conditions and Thermo-Calc provided the thermodynamic information needed (Fig. 4). First a thermodynamic study was performed with Thermo-Calc by using the COST2 [22] data base. This data base provides the thermodynamic data for the ternary phase diagram Zn-Al-Mg [23]. Within the Zn rich corner of the ternary system four phases might exist, the hexagonal close packed (hcp) Zn-phase, the face centered cubic (fcc) Al-phase, the Laves-C14 $MgZn_2$ phase and the intermetallic Mg_2Zn_{11} phase. A ternary eutectic exists at the concentration of 3.9 wt.% Al and 2.4 wt.% Mg [24].

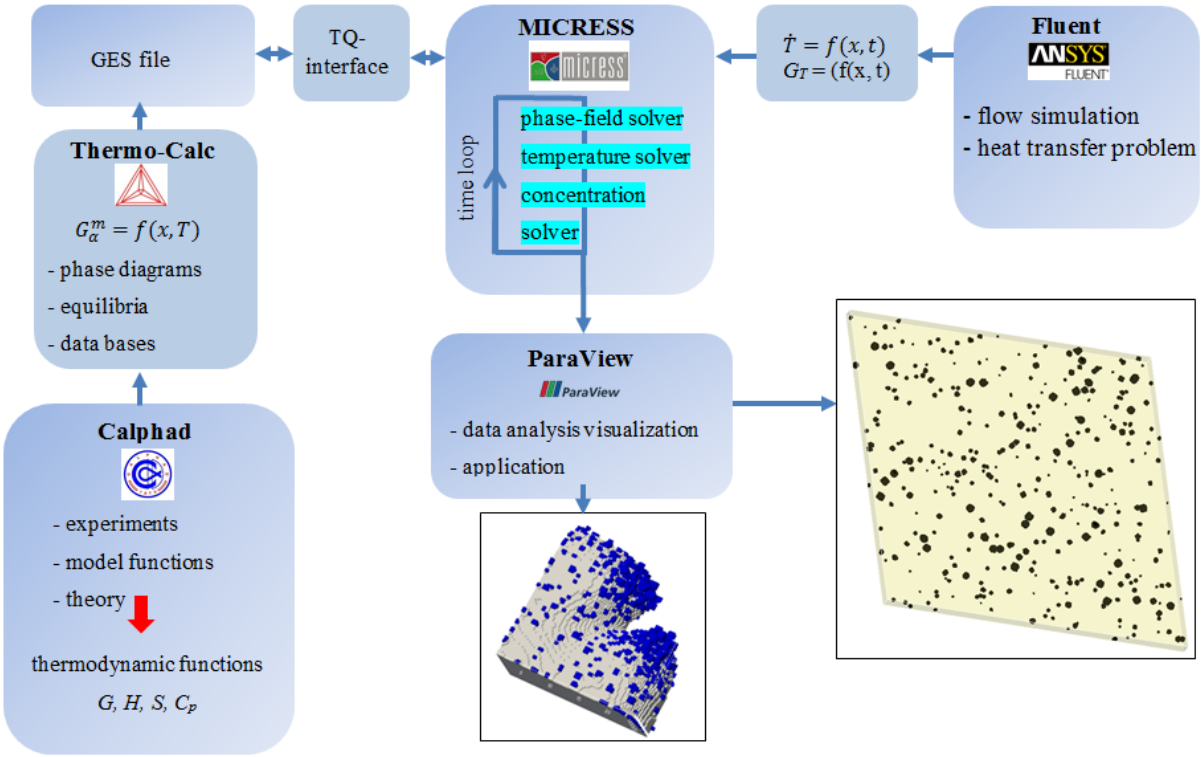

Figure 4: Overview of software being coupled

By using the database COST2 it is possible to calculate the phase equilibria of Zn-Al-Mg alloys as a function of compositions and temperatures. Calculations were made for the ternary phase diagram at different temperature levels, and amounts of phases considering a Scheil-type solidification approach for selected concentrations were estimated. Since the phase Mg_2Zn_{11} occurs only in equilibrium, this phase was erased from the calculations. For Zn-2.5

[3] http://www.ansys.com/Products/Fluids/ANSYS-Fluent
[4] http://www.paraview.org/

wt.% Al- 1.5 wt.% Mg the results of such a ternary solidification simulation is shown in Fig. 5a.

Approximately, 45 wt.% of the total solid is supposed to consist of the primary Zn-phase which starts to solidify at ~373 °C. Only 3 wt.% of a binary eutectic (consisting of Al- and Zn-phase) which starts at 340 °C is predicted. The remaining liquid solidifies at 336 °C as ternary eutectic by adding the $MgZn_2$ phase to the binary eutectic. The corresponding temperature depending amount of phase fractions is shown in Fig. 5b. In solid state the microstructure consists of 82 wt.% Zn-phase, 8.9 wt.% $MgZn_2$-phase, and 9.1 wt.% Al-phase.

In order to estimate the macroscopic temperature field in the coating, the sample within the GalvaSim was cooled down after the coating and the corresponding sheet temperature was recorded. The geometry of the steel sheet and the cooling aggregates were mapped into ANSYS-FLUENT. The unknown radiation heat flux of the sample was adopted in such a way to obtain an equal temperature trend as for the GalvaSim experiments. Additionally, the time-depending temperature gradient within the zinc layer normal to the surface was numerical estimated (Fig. 6). As a result a file was created for further used with MICRESS where corresponding temperatures, cooling rates, and temperature gradients as function of time were listed.

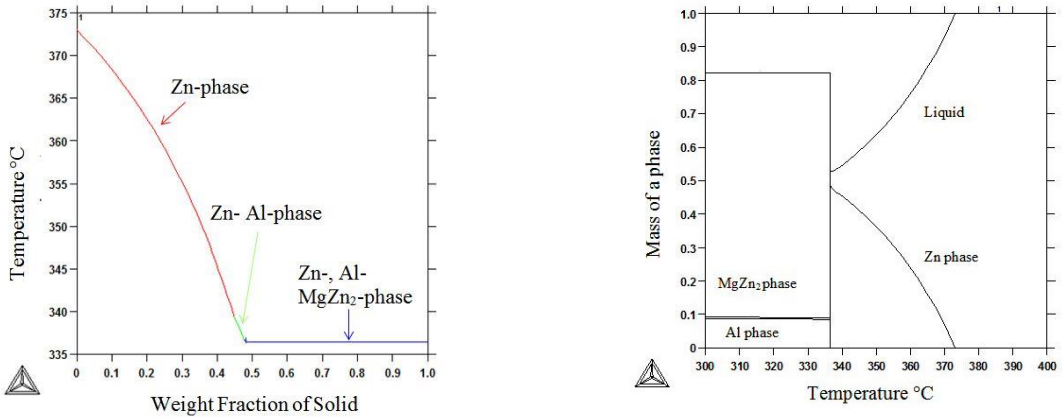

(a) (b)

Figure 5: (a) Increase of solid fraction with temperature based on a ternary Scheil calculation and (b) corresponding evolution of phase fraction as function of temperature for an Zn-2.5 wt.% Al- 1.5 wt.% Mg alloy.

The numerical investigation with MICRESS is divided into three different topics, the nucleation events, the investigations on the binary eutectic and on the lamellae structure of the ternary eutectic. The used physical parameters are given in Table 1.

Table 1: parameters

surfaces energy $\sigma_{s,l}$	$1 \cdot 10^{-2}$	J/m^2
diffusion coefficient in the liquid D_L	$1 \cdot 10^{-9}$	m^2/s
diffusion coefficient in the solid D_s	$1 \cdot 10^{-13}$	m^2/s

The boundary conditions like cooling rate and temperature gradient were read from a file created by ANSYS-FLUENT and based on the experimental data from GalvaSim. The observation of the nucleation of the primary Zn-phase requires a domain which gives a sufficient overview of the coating layer in order to be meaningful. To do so the selected domain is in the order of 280x280x10 μm^3 in size, meshed with around 1.5 million cubic cells with 0.8 µm edge length. As time step we have used $\Delta t = 0.1$ s.

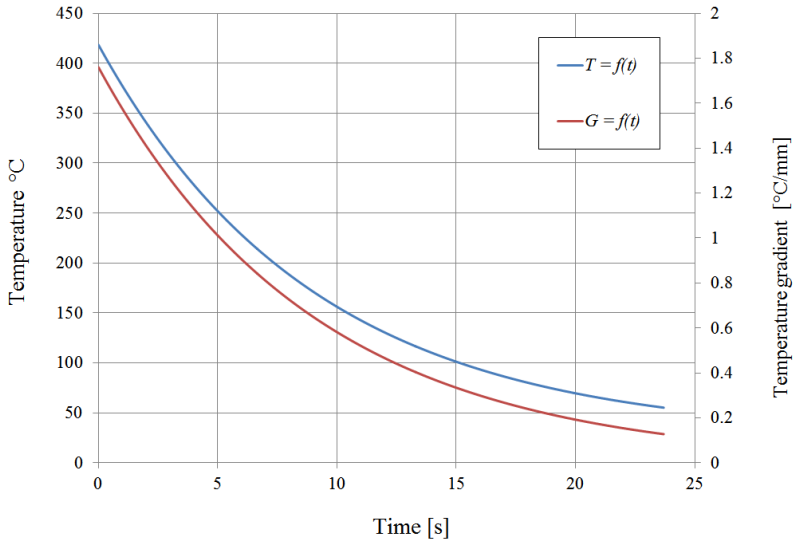

Figure 6: Cooling curve and temperature gradient (normal to surface) calculated by numerical investigation of the macroscopic temperature field in the steel sheet and the coating as to match corresponding GalvaSim results.

As up to now no quantitatively accurate model for describing heterogeneous nucleation of non-inoculated alloys in technical situations exists, MICRESS offers a semi-empirical approach named “seed density model” [17]: A predefined amount number density of possible potential nuclei as seeds are discretely positioned within the domain. They can be divided into different classes with a defined range of effective critical radii and corresponding seed number densities. In this work we have used seven seed classes. Based on the Gibbs-Thomson equation and by knowing the surface energy, σ_{sl}, and the solidification entropy, S_f, the program calculates the undercooling, ΔT_u, necessary to create critical nuclei of the definite size. So, to activate a given size class a certain undercooling is needed. Note that large nuclei need less undercooling and note that the actual undercooling temperature might not be constant within the domain as microsegregation during solidification leads to locally different liquidus temperatures. Since the liquid coating layer is forced to cool and solidify by using cooling aggregates, and the corresponding cooling rates and temperature gradients were calculated macroscopically by ANSYS-FLUENT (Fig. 6), the time-dependent temperature distribution within the domain was known. Fig. 7 gives an example of the corresponding evolution of the nucleation process for the primary Zn-phase. Here, we have applied no-flux boundary conditions at the top and bottom faces and periodic boundary conditions at the side faces.

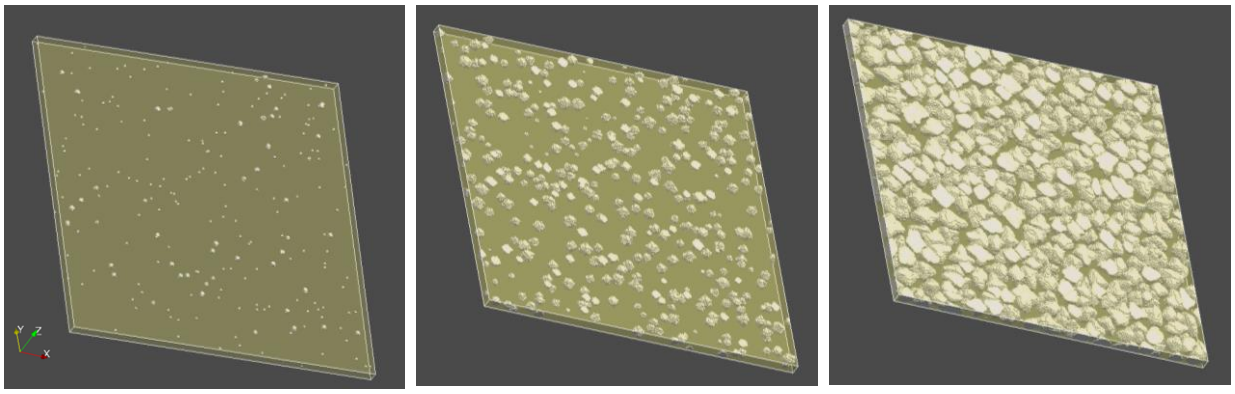

$t = 0.015$ s $t = 0.0335$ s $t = 0.0341$ s

Figure 7: Sequence of nucleation events for the primary Zn-phase in a coating cooled by cooling rates and temperature gradients as given in Fig. 6. The simulated area was 280 µm in width and length with a thickness of 10 µm. 1.5 million numerical volume elements were considered.

While only liquid was present at $t = 0$ s, first nuclei are activated as soon as the local undercooling close to the melt surface exceeds the critical undercooling of the biggest seeding particles as defined by the chosen seeding classes and local temperature. During further cooling these activated nuclei start growing (Fig. 7a). With increasing undercooling, the following seed classes are activated (Fig. 7b). Nucleation is finished as soon as all potential seeds have been activated or have been shielded by neighboring grains as a consequence of segregation or overgrowth (Fig. 7c).

The selected size of the domain allows for a comparison of the final grain structure to experimental observations (Fig. 3a, b) but is insufficient for investigation of the solidification pattern in the eutectic regions. Detailed investigations of the nucleation event for the eutectic required a higher resolution. In order to do so a smaller section of the coating layer from Fig. 7 that contains quarter of a Zn-dendrite as shown in Fig. 8a was selected. Now the domain was 25x25x10 μm^3 in size meshed with around 0.4 million cubic cells with 0.25 µm edge length. For the example shown in Fig. 8, we have used no-flux boundary conditions for the top and bottom faces and symmetry boundary conditions for the side faces with a time step of $\Delta t = 0.05$ s. For the nucleation of the Al- and $MgZn_2$ phase we have applied the "undercooling model" model [28] rather than the "seed density model". The "undercooling model" considers nucleation at a certain undercooling (we have assumed 10 K for the results in this paper) and sets randomly as much nuclei of critical size as possible whereby a predefined minimum distance between the nuclei had to be kept.

The nucleation and growth of the eutectic takes place in three stages. First, nucleation of the Al phase happens mainly on "secondary arms" (Fig. 8b) while the Al-phase continues to growth. Thus, a binary eutectic forms here and there, while the Al-phase continues to nucleate (Fig. 8c). Then, the $MgZn_2$ phase nucleates all over the entire dendritic surface (Fig. 8d) and the competitive growth of all three phases (Fig. 8e) leads to the lamellae growth of the ternary eutectic (Fig. 8f). However, a detailed study of the coupled ternary eutectic growth needs again an even finer grid.

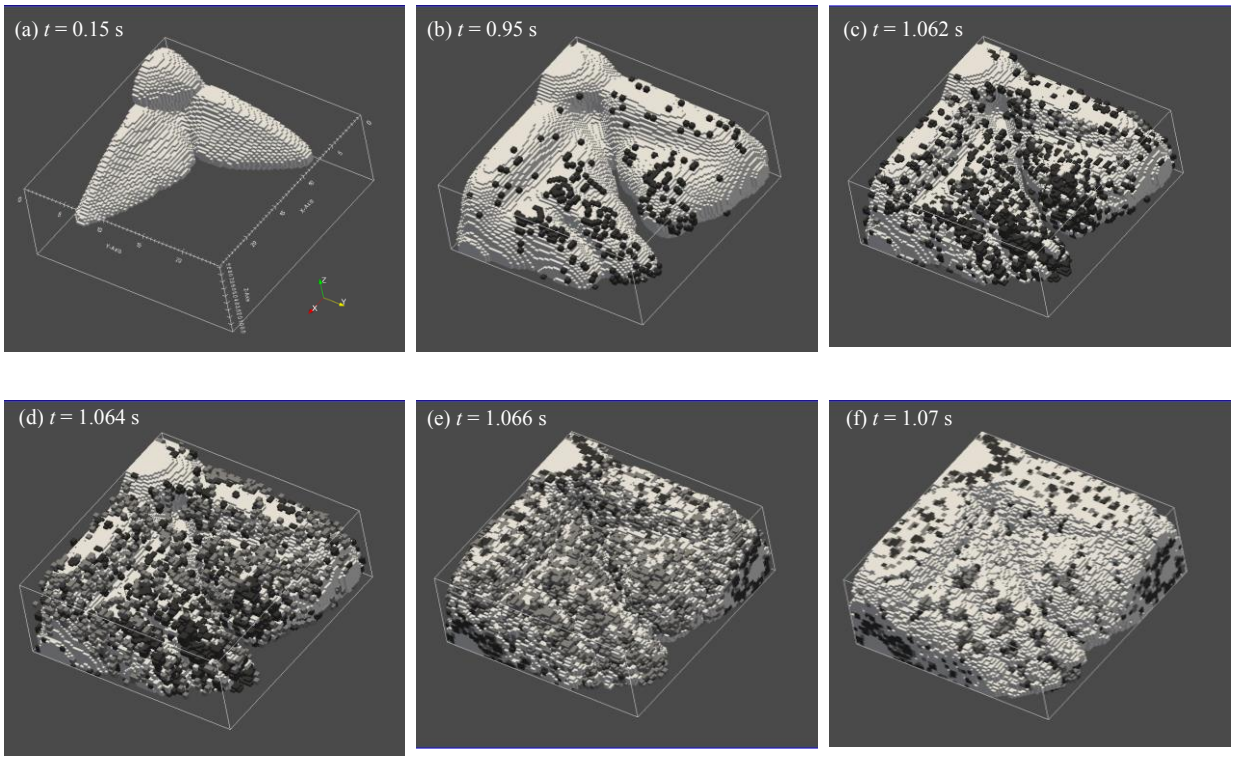

Figure 8: Sequence of nucleation and growth for the binary and ternary eutectic: (a) Segment of a Zn-phase dendrite, (b) and (c) nucleation of the Al-phase (black dots), (d) nucleation of the $MgZn_2$-phase (gray dots), and (e and f) growth of the ternary eutectic.

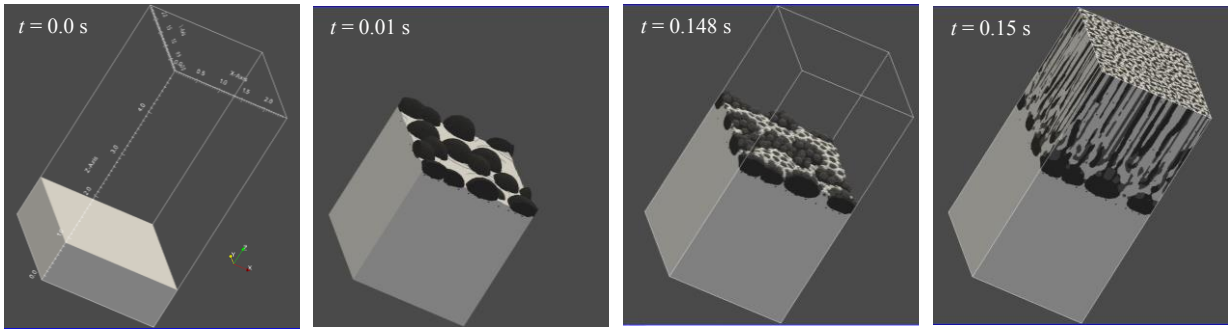

(a) (b) (c) (d)

Figure 9: Formation of the binary and ternary eutectic. (a) surface section of the preexisting zinc phase, (b) nucleation of the Al phase at the zinc surface, (c) nucleation event of the $MgZn_2$ phase, and the solidification pattern of the ternary eutectic.

For a further study of nucleation and growth of binary and ternary eutectic, a domain as small as 2.5x2.5x5 μm^3 was considered. The cubic cells of the numerical grid had an edge length of 12.5 nm, so that the grid consisted of 16 million volume elements. As time step we have used $\Delta t = 0.001$ s. As boundary conditions we applied again no-flux boundary conditions at the top and bottom faces and periodic boundary conditions at the side faces. The starting point of the simulation was now a smaller surface area of a Zn-dendrite represented by a preexisting rectangle grain (Fig. 9a). During cooling the Zn- phase grows until the first Al-phase nuclei occurred at the dendritic surface (Fig. 9b). After a while, the $MgZn_2$ phase nucleated (Fig. 9c)

and the binary eutectic was overgrown by a coupled ternary eutectic (Fig. 9d).

4 DISCUSSIONS

It is theoretically conceivable to simulate the whole sequence of solidification in only one simulation. For that the plate-like domain (280x280x10 μm^3) shown in Fig. 7 would have to be meshed with volume elements as small as 12.5x12.5x12.5 nm^3. That would result in a mesh of 3.2 10^{11} volume elements – 4-5 orders of magnitude larger than what can be processed with modern HPC computers. Therefore, a partitioning in different length scale simulations cannot be avoided.

Ternary Scheil-type solidification simulations (1D without any nucleation) based on Thermo-Calc in combination with the COST2 data base for the Zn-Al-Mg system give already a reasonable idea of the phases that form (as long as the sluggish equilibrium phase Mg_2Zn_{11} is omitted). However, for the exact solidification path (especially when the amount of Al in the ternary alloy is slightly decreased and the binary eutectic changes from fcc-Al/ hcp-Zn/liquid to $MgZn_2$/hcp-Zn/liquid), nucleation and three dimensional morphology development including solute diffusion has to be considered.

A specific experimental feature is the occurrence of the edge of dots of Al- and $MgZn_2$-phase that surround the primary Zn-phase (Fig. 3b). This can be attributed to nucleation of (in the present case first) the Al-phase and (shortly after) of the $MgZn_2$-phase in direct contact with the Zn-phase (Fig. 8d and 9c). Having this configuration, the ternary Zn/Al/ $MgZn_2$-eutectic growth in a coupled and lamellar manner. From the experimental observation (Fig. 3c) it is not clear whether especially the Al-phase forms continuous lamellae or repeatedly nucleates and grows as isolated globular crystals. We have intensively varied the nucleation conditions for the Al-phase ahead of the eutectic front but we could not get ternary eutectic microstructures that resemble the experimental ones. In fact, couple lamellar growth (as the one shown in Fig. 9d) establishes quite automatically and under various conditions. We rather think that the globular appearance of the fcc-Al phase at room temperature may be connect to the afore mentioned solid/solid decomposition. However, the experimental appearance of the ternary eutectic depends quite dramatically on the chosen cross section of the sample. Fig. 10a shows a cross section taken perpendicular to the growth direction and Fig 10b a cross section with same arbitrary inclination.

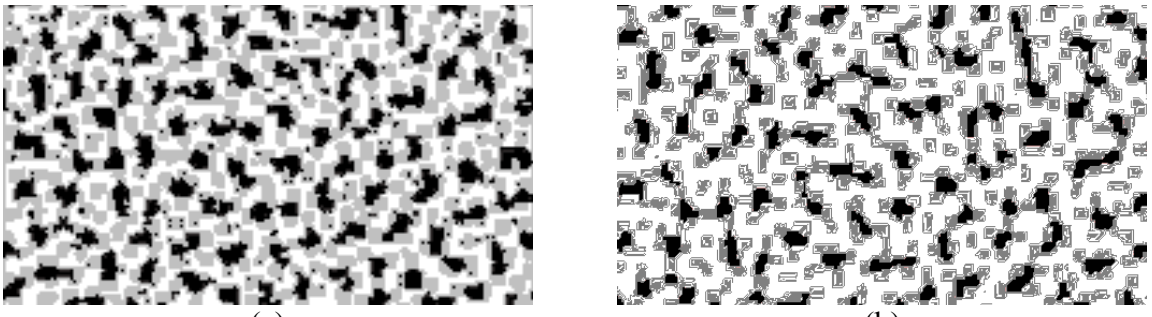

(a) (b)

Figure 10: Cross section through the numerically calculated ternary eutectic taken perpendicular to the growth direction (a) and at some arbitrary inclination (b).

The comparison between experimental observations and numerical predictions for the ternary eutectic is thus done by estimating the phase amount (and length scales) on different cross sections taken at various inclinations (numerical results) and different eutectic grains (experimental results). Table 2 shows the corresponding mean area fractions with standard derivation. Obviously both results match to some extent. In the light of the complexity of the current solidification process the agreement is satisfactory.

Table 2: Amount of phases

	numerical result		experimental result	
phase	area [%]	error bar	area [%]	error bar
Zn	50.9	± 4.6	45.9	± 5.1
Al	18.0	± 5.7	14.6	± 2.4
MgZn2	31.1	± 1.6	39.5	± 7.0

5 CONCLUSIONS

In the present work, we have demonstrated that it is possible to numerically simulate the microstructure formation on solidification of a Zn-2.5 wt.% Al-1.5 wt.% Mg alloy during hot dip galvanization. However, the challenge is that cooling of the coated steel sheets happens on a meter length scale, growth of primary dendrites on a micrometer length scale and nucleation and growth of binary or ternary eutectic on a sub-micrometer length scale. In addition, thermodynamic phase diagram information for the ternary Zn-Al-Mg system must be taken into account on any length scales. Thus, four different process simulations (ANSYS-FLUENT, MICRESS) on different length scales were combined with each other and with a thermodynamic program (Thermo-Calc) that uses information from a specific data base (COST2). In order to match experimental observations, especially the nucleation parameters for three solid phases involved (fcc-Al, hcp-Zn, and $MgZn_2$) were chosen adequately. Although a parameter-free model would be desirable, solidification processes that are govern to a large extend by nucleation (as in the present case) can yet not be described by first principles.

6. ACKNOWLEDGEMENT

Financial support has been provided by the Austrian Federal Government (in particular from Bundesministerium für Verkehr, Innovation und Technologie and Bundesministerium für Wissenschaft, Forschung und Wirtschaft) represented by Österreichische Forschungsförderungsgesellschaft mbH within the framework of the COMET Funding

REFERENCES

[1] Raghavan, V. Al-Mg-Zn (Aluminum-Magnesium-Zinc). *Journal of Phase Equilibria and Diffusion* (2007) **28**: 203-208.

[2] Yu, K., Li, J. Liu, X., Li, J. and Xue, X. Microstructure of Hot-Dip Galvanized Zn-Al-Mg Alloy coating. *J. Shanghai Jiaotong Univ.* (2012) **17**: 663-667.

[3] Marder, A.R. The metallurgy of zinc-coated steel. *Progress in Materials Science* (2000) **45**: 191-271.

[4] https://www.andritz.com/me-hotdipgalvanizinglineno4-brochure_en.pdf.
[5] Tsujimura, T., Komatso, A. and Andoh A. *Influence of Mg content in coating layer and coating structure on corrosion resistance of hot-dip Zn- Al- Mg alloy coated steel sheet.* Galvatech' 01, (2001) 145-152.
[6] De Bruycker, E. *Zn-Al-Mg Alloy Coatings: Thermodynamic analysis and microstructure-related properties.* University Genf, (2006).
[7] Liu, H.Y. and Jones, H. Solidification microstructure selection and characteristics in the zinc-based Zn-Mg System. *Acta Metall. Mater.* (1992) **40:** 229-239.
[8] Akdeniz, M.V. and Wood J.V. Microstructure and phase selection in rapidly solidified Zn-Mg alloys. *J. Mater Sci.* (1996) **31:** 545-550.
[9] Bluni S.T., Marder, A.R. Improvement of Galfan surface appearance for coil coating uses. *4th Int. Zinc Coated Sheet Conf., Paris, France,* (1994) SC6/1. 15.
[10] Lamberights, M. and Leroy, V. ZM-285 Progress Report, ILZRO, (1991) **23**.
[11] Coutsouradis, F.E. Goodwin, J. Pelerin, A.F. Skenazi, A. and Davin XY. Latest developments of Galfan protective coatings. *Stahl und Eisen* (1984) 104: 1073-1080.
[12] Pelerin, J. Bramaud, B. Nouville, J.F. Coutsouradis, D. Herrschaft, D.C. and Radtke, S.F. GALFAN: A new Zninc-Aluminium coating. Part I: Zinc-5% Aluminium-Mischmetall coated sheet. *Proc. 13th Int. Galvanizing Conf., London, UK,* (1982) 49/I.
[13] Tiaden J, Nestler B, Diepers HJ, Steinbach I. Physica D 1998; 115:73.
[14] Boettinger, W.J. Warren, J. Beckermann, C. and Karma A. Phase-field simulation of solidification. *Annu. Rev. Mater. Res*. (2002) **32**: 163-94.
[15] Moelans, N. Blanpain, B. and Wollants P. An introduction to phase-field modeling of microstructure evolution. *Computer Coupling of Phase Diagrams and Thermochemistry* (2008) **32**: 268-294.
[16] Eiken J, Böttger B, Steinbach I. Phys Rev E 2006; 73:066122.
[17] Böttger, B. Eiken, J. and Steinbach, I. Phase field simulation of equiaxed solidification in technical alloys. *Acta Mater.* (2006) **54**: 2697-2704.
[18] Böttger B, Eiken J, and Apel M, Comput. Mater. Sci. 108, 283 (2015).
[19] Eiken, J. Phase-field simulation of microstructure formation in technical magnesium alloys. *Int. J. Mater. Res.* (2010) **101**: 503-509.
[20] M. Apel, B. Böttger, H.-J. Diepers, I. Steinbach: 2D and 3D phase-field simulations of lamellar and fibrous eutectic growth. Journal of Crystal Growth 237-239 (2002) p.154-158.
[21] Tragl, E. Strutzenberger, J. Angeli, G. Pichler, A. Faderl, J. and Haunschmid, H. *Simulators for product- and process development of new steel grades*. Metal (2005). 14th Int. Metall. Mater. Conf., Hradec and Moravici, CZ, 24.-26.5.2005.
[22] European Commission and technical research *Definition of thermochemical and thermophysical properties to provide a database for the development of new light alloys.* COST European cooperation in the field of scientific (1998) **2**: ISBN 92-828-3902-8.
[23] Liang, P. Tarf, T. Robinson, J.A. Wagner, S. Ochin, P. Harmelin, M.G. Seifert, H.J. Lukas, H.L. and Aldinger F. Experimental investigation and thermodynamic calculation of the Al-Mg-Zn system. *Thermochimica Acta* (1998) **314:** 87-110.
[24] De Bruycker, E. Zermout, Z., and De Cooman B.C. Zn-Al-Mg Coating: Thermodynamic analysis and microstructure related properties, *Mater. Sci. Forum* (2007) **539-543**: 1276-1281.